CELLULAR LOGISTICS
2017, VOL. 7, NO. 3, e1361499 (14 pages)
https://doi.org/10.1080/21592799.2017.1361499

Taylor & Francis
Taylor & Francis Group

RESEARCH PAPER

Intermolecular interactions involving an acidic patch on immunoglobulin variable domain and the γ2 constant region mediate crystalline inclusion body formation in the endoplasmic reticulum

Haruki Hasegawa [a], Mei Geng[a], Randal R. Ketchem [a,*], Ling Liu[b], Kevin Graham[b], and Frederick Jacobsen [b]

[a]Department of Therapeutic Discovery, Amgen Inc., South San Francisco, CA, USA; [b]Department of Therapeutic Discovery, Amgen Inc., Thousand Oaks, CA, USA

ABSTRACT

Full-length immunoglobulins (Igs) are widely considered difficult to crystallize because of their large size, N-linked glycosylation, and flexible hinge region. However, numerous cases of intracellular Ig crystallization are reported in plasma cell dyscrasias. What makes some Ig clones more prone to crystallize during biosynthesis as well as the biochemical and cell biological requirements for this cryptic event are poorly understood. To investigate the underlying process of intracellular Ig crystallization we searched for model IgGs that can induce crystalline inclusions during recombinant overexpression. By testing various subunit combinations through mixing and matching of individual subunit chains derived from a panel of human IgG clones, we identified one secretion competent IgG2λ that induced needle-like crystalline inclusions in transfected HEK293 cells. Ig crystallization rarely occurred at steady-state cell growth conditions but was easily induced when ER-to-Golgi transport was pharmacologically blocked. Homology modeling revealed the presence of a prominent negatively-charged patch on the variable domain surface. The patch was composed of eight aspartic acids, of which five were in the heavy chain variable region and three were in the light chain. Crystallization occurred only when the two subunits were co-transfected and the intracellular crystals co-localized with ER resident proteins. Furthermore, subtype switching from IgG2 to IgG1 and stepwise neutralization of the acidic patch independently abrogated Ig crystallization events. The evidence supported that the formation of needle-like crystalline inclusions in the ER was underscored by multivalent intermolecular interactions between the acidic patch and undefined determinants present on the γ2 subunit constant region.

ARTICLE HISTORY
Received 28 June 2017
Revised 24 July 2017
Accepted 25 July 2017

KEYWORDS
acidic surface patch; crystalline body; endoplasmic reticulum; immunoglobulin; morular cell phenotype; Russell body

Introduction

The tractable first report on intracellular protein crystallization event was published in 1917 by Glaus on multiple myeloma cells.[1] Extensive immunohistological studies revealed that the crystals occurring within the cytoplasm of plasma cells were composed of assembled immunoglobulins (Igs) or free subunit chains.[2-4] Although numerous cases of intracellular Ig crystallization events have been documented to date in a variety of human clinical samples associated with plasma cell dyscrasias, the studies were mainly driven by "morphologic curiosity"[5] and did not typically go beyond reporting the crystal morphology, determining the isotypes of involved Ig species, or identifying amino acid substitutions in the complementarily-determining regions (CDRs).[6] Nonetheless, accumulation of electron microscopy data unequivocally showed that crystals were housed in the ribosome-studded rough endoplasmic reticulum (ER).[7-13] These findings implicated that the Ig crystallization events were associated with biosynthetic activities of plasma cells. It is important to note that the crystalline inclusions reported in crystal-storing histiocytosis[14] and pseudo-Gaucher cells[15] were of different origins in that the Ig crystals were stored in the lysosomes of macrophages and plasma cells, respectively, as a result of impaired intra-lysosomal degradation. Notably, after 100 years from the first report, the underlying molecular determinants and cell biological requirements leading to the formation of intracellular Ig crystals are still not well understood.

One important clue to understand the biochemical basis of intra-ER antibody crystallization came from the work of Rengers et al. (2000)[16] where they investigated the spontaneous Ig crystallization event in hybridoma cells expressing a mouse monoclonal IgG3κ clone 8A4. Rengers et al. noticed that two variants of 8A4 hybridoma lost crystalline inclusion formation and found out that the crystal loss was independently caused by 3-amino acid deletion in the Vκ or the HC subtype switching to IgG1.[16] Based on these observations, Rengers et al. proposed that sequence-encoded properties within the variable and constant domains of both subunits were responsible for the intracellular crystallization of 8A4 mAb.[16] Additional insights came from the studies of Hasegawa et al.[17] in which the authors identified and characterized a human IgG2κ mAb that induced crystalline inclusions in the ER during recombinant overexpression. One of the hallmark

CONTACT Haruki Hasegawa PhD harukih@amgen.com Amgen Inc. 1120 Veterans Blvd, South San Francisco, CA 94080, USA.
*Current address: Just Biotherapeutics, Seattle, WA, USA

characteristics of this IgG2κ mAb was the presence of a negatively-charged cluster consisting of five aspartic acid residues on the surface of variable domain.[17] Neutralization of this acidic patch abolished the mAb's crystallizing propensity at the neutral pH environment of the ER lumen.[17] Transient expression studies using HEK293 cells demonstrated that even when the IgG had high intrinsic propensities to crystallize, intra-ER crystal nucleation did not take place unless the export-ready IgG accumulated above a threshold concentration.[17] Because different cell types tend to have different capacities for protein synthesis, folding and transport, the threshold concentration can be reached spontaneously in some cell types, while a blockade of ER-to-Golgi transport may be required in others.[17,18]

To obtain mechanistic insights into the intra-ER crystallization of Ig molecules, we investigated the molecular determinants and the nature of underlying protein–protein interactions that make some mAbs crystallize in the ER. After mixing and matching of various antibody subunit chain panels, we identified a secretion competent model human IgG2λ mAb that induced crystalline inclusion bodies resembling a stack of fine needles. Because of the non-cognate HC–LC pairing, the identified human IgG2λ had no known antigen specificities or biologic functions. Homology modeling revealed that the model IgG2λ possessed a prominent acidic surface patch on the variable domain because of the sequence characteristics embedded in the assembling γ2-HC and λ-LC subunits. Crystallization required an accumulation of assembled IgGs to reach a certain threshold concentration in the ER. In the employed HEK293 expression system, such concentration was achieved after brefeldin A treatment. Individual subunit chains by themselves were secretion incompetent and were not able to induce crystalline inclusion bodies. Furthermore, the disruption of acidic patch and the subtype switching from γ2 to γ1 independently abrogated the crystallizing propensity. Collectively, the evidence supported that the intra-ER crystallization event was underscored by multivalent intermolecular interactions involving the negative charge patch on the variable domain and undefined elements present within the γ2-HC constant domain.

Results

Identification of a secretion competent human mAb that has a prominent acidic surface patch consisting of eight aspartic acids.

By using the cell phenotype screening assay we developed previously,[18] we set out to identify a group of model mAbs that can induce intracellular crystalline inclusion bodies. By mixing and matching of the HC and LC subunits from a panel of human IgG mAbs, we identified one such human IgG mAb denoted as mAb-3 (see Fig. 1A). The mAb-3 is consisted of a human γ2-HC subunit that has five aspartic acid residues in CDR3 and a human λ-LC subunit that has three aspartic acids in CDR2. Coincidentally, the HC subunit was derived from a previously-investigated human IgG2κ (denoted as mAb-1 in Fig. 1A) that readily formed rod-shaped crystalline inclusions in the ER when paired with its cognate κ-LC [17]. The LC subunit, on the other hand, was derived from a human IgG2λ mAb (denoted as mAb-2 in Fig. 1A) that was previously shown to exhibit high viscosity problems [19]. Because the HC and LC subunits originated from two distinct IgGs that recognized two unrelated antigens, the resulting mAb-3 had no known antigen specificity or biologic function. Homology modeling of the mAb-3 variable fragment (Fv) illustrated that all eight aspartic acid residues in the CDRs contributed to form a large acidic surface patch (estimated ~660 Å^2) on the variable domain (Fig. 1 BC). The isoelectric point of mAb-3 was predicted to be pH 6.63 (see Table-1).

To ensure the mAb-3 is a suitable model that supports correct folding, assembly and secretion, we next examined its secretion competency by using a HEK293 cell transient expression system. By co-expressing the γ2-HC and λ-LC subunits, 277.3 $\pm$ 52.3 mg/L (n = 18) of mAb-3 was secreted to the cell

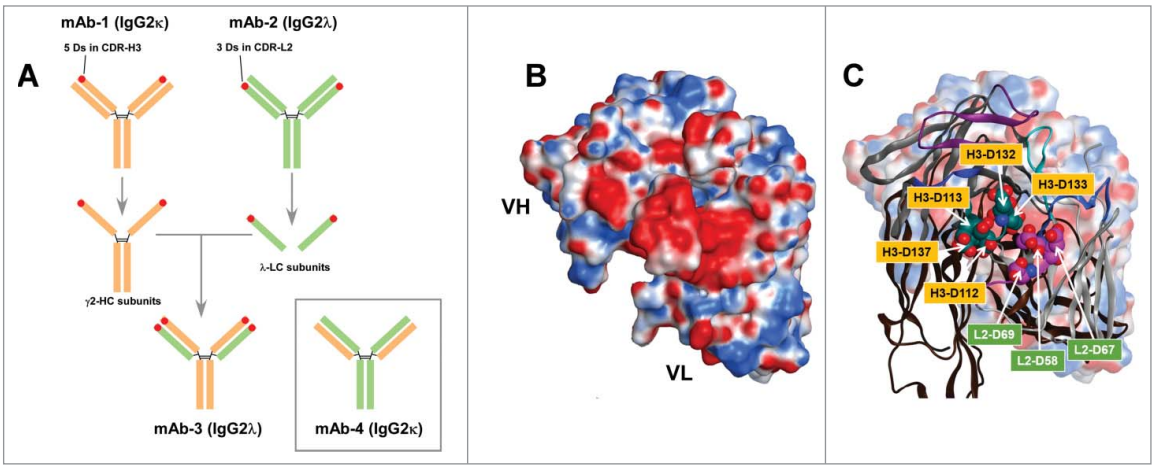

Figure 1. Generation of a model human IgG mAb-3 possessing an acidic patch on the variable domain surface. (A) Schematic depiction of model mAbs. Two antibodies shown at the top are mAb-1 (IgG2κ) colored in orange and mAb-2 (IgG2λ) in green. Red circles located on the mAb-1's HC and mAb-2's LC represent the areas where negatively charged amino acids are densely located. Five Asp residues are in mAb-1 CDR-H3. Three Asp residues are in mAb-2 CDR-L2. The mAb-1 γ2-HC was paired with the mAb-2 λ-LC to generate mAb-3. Similarly, the mAb-1 κ-LC was paired with the mAb-2 γ2-HC to generate mAb-4 (shown in box). (B) A homology model showing the variable fragment of mAb-3. The surface is color-coded by the underlying amino acid residue charge in which red is negative, blue is positive, and white is neutral. VH, heavy chain variable domain. VL, light chain variable domain. (C) An overlay of the surface model and a corresponding ribbon diagram. Individual Asp residues comprising the prominent acidic patch are shown with the respective residue using the AHo numbering system[33]. Asp residues on CDR-H3 are shown in yellow background, while Asp residues on CDR-L2 are shown in green background.

Table 1. Selected physicochemical properties of human IgG mAbs.

Model antibody	Predicted isoelectric point	Intracellular CB formation in HEK293	CB formation required BFA treatment	Spontaneous CB induction in stable CHO cell line	CB morphology	Reference
mAb-1	7.05	Yes	Yes	Yes	thick rod	[17] & This study
mAb-1 (G1 version)	8.09	No	—	—	—	unpublished data
mAb-1 (HC-D>A)	8.54	No	—	—	—	[17]
mAb-2	7.84	No	—	—	—	[19] & This study
mAb-3	6.63	Yes	Yes	—	stack of fine needles	This study
mAb-3 (G1 version)	7.16	No	—	—	—	This study
mAb-3 (HC-D>A)	7.78	No	—	—	—	This study
mAb-3 (LC-D>A)	7.13	No	—	—	—	This study
mAb-3 (HC-D>A/LC-D>A)	8.57	No	—	—	—	This study
mAb-4	8.60	No	—	—	—	This study
IgG1λ	8.75	Yes	Yes	—	long sharp needle	[18]
IgG2λ	8.36	Yes	Yes	Yes	grain	[18]
IgG2λ (N297A)	8.36	No	—	—	—	[18]
IgG3λ	8.80	No	—	—	—	[18]
IgG4λ	8.08	Yes	No	—	short thick needle	[18]
Fab	8.66	Yes	Yes	—	thin long rod	[18]

Note. –, not determined; CB, crystalline body; BFA, Brefeldin A;

culture medium in a 7-day batch cell culture process (Fig. 2A, lanes 1 and 7; Fig. 2C, lanes 1 and 5; Fig. 2D, lanes 1 and 3). When the culture medium sample was analyzed under non-reducing conditions, the HC and LC assembled primarily into ~150 kDa species, as expected, but additional bands such as ~300 kDa, ~140 kDa and 110 kDa were also observed (Fig. 2A, lane 7; Fig. 2C, lane 5). The presence of heterogeneous species was somewhat expected due to known heterogeneity in the inter-chain disulfide bond connectivity for human IgG2s.[20] We point out here that the polysera used to detect human IgGs by Western blotting gave disproportionately weaker signals for λ-LCs comparted to those of κ-LCs or HCs (see Fig. 2 CD, lanes 1–2; also shown previously in[18]). Similar to many other HC subunits, HC alone was not secreted to the culture medium, although the protein was synthesized in the cells (Fig. 2A, lanes 2, 5, 8). While LCs are typically secreted to the culture medium as a mixture of monomers and covalently-linked dimers in the absence of HC synthesis[17,18,21] (see also Fig. 2C, lanes 4, 8, 12), this model LC subunit was unusual in that the LC-only secretion was barely detectable despite the LC synthesis (Fig. 2A, lanes 3, 6, 9).

Mixing and matching of the individual subunit chains between mAb-1 and mAb-2 can generate another IgG mAb (denoted as mAb-4 in Fig. 1A, box). The mAb-4 was also secretion competent with a 7-day production titer of 299.1 ± 28.4 mg/L (n = 6) (Fig. 2C, lanes 2, 6, 10; Fig. 2D, lanes 2, 4). The individual subunit chains that comprise mAb-4 behaved expectedly. Namely, the LC alone was secreted as a mixture of monomers and covalent dimers (Fig. 2C, lanes 4, 8, 12), while the HC alone was not secreted (Fig. 2C lanes 3, 7, 11). Unlike the case of mAb-3 (see below), mAb-4 did not produce any notable cell phenotypes during recombinant overexpression in HEK293 cells (data not shown).

Model mAb-3 induces crystalline inclusion bodies resembling a stack of needles in HEK293 cells when ER-to-Golgi transport is blocked.

After its secretion competency was confirmed, we next asked if mAb-3 can induce CBs. Under steady-state normal cell growth conditions, immunofluorescent microscopy revealed that intracellular mAb-3 distributed to the ER and Golgi when both subunits were individually visualized, and there was no detectable CB formation (Fig. 3A). Our previous studies[17-18] implicated that secretion competent IgGs may not always accumulate to a high enough concentration in the ER to reach a crystallizing threshold in transiently transfected HEK293 cells. To overcome this issue, we treated the cells with brefeldin A (BFA) to block ER-to-Golgi transport (see Fig. 2B) and withheld the export-ready IgG species in the ER. After 24 hr of BFA treatment, from day-2 to day-3 post transfection, approximately 17% of transfected cells (39 CB-positive cells/229 transfected cells) developed CBs that resembled a stack of fine needles (Fig. 3B, arrowheads). Unlike the CB phenotypes induced by two previously characterized human IgG clones,[17,18] mAb-3 CBs were not readily discernible even with a DIC microscope. Furthermore, depending on the needle orientation, some CBs were difficult to detect. As a result, determining the accurate count of CB phenotype frequency in a population of transiently transfected HEK293 cells was not straightforward, especially when thin needles were not in the plane of focus. Accordingly, the phenotype percentage reported above can be lower than the actual percentage due to undercounting.

Similar to the cases of previously reported CBs,[17,18] the polysera against individual subunit chains did not penetrate into the CBs to stain them directly (Fig. 3B). This was somewhat expected because the protein crystals were formed as a result of liquid-solid phase separation, and the goat polysera could not simply penetrate into the interior of crystalline objects made of human IgG lattice. Nonetheless, in order to demonstrate these needle-like inclusions were made of mAb-3 proteins (but not of cellular proteins or salts) while simultaneously circumventing these molecular packing issues, we probed these thin needles with two different detection reagents smaller than the size of antibodies. The first probe was a fluorescent-conjugated Fab fragment (~50 kDa) generated from goat anti-human IgG (H + L) polysera. The second was a fluorescent-conjugated Protein A (~42 kDa). These two probes were able to label the needle-like CBs effectively—and demonstrated the immunoglobulin nature of CBs (Fig. 4A). Furthermore, the needle-like

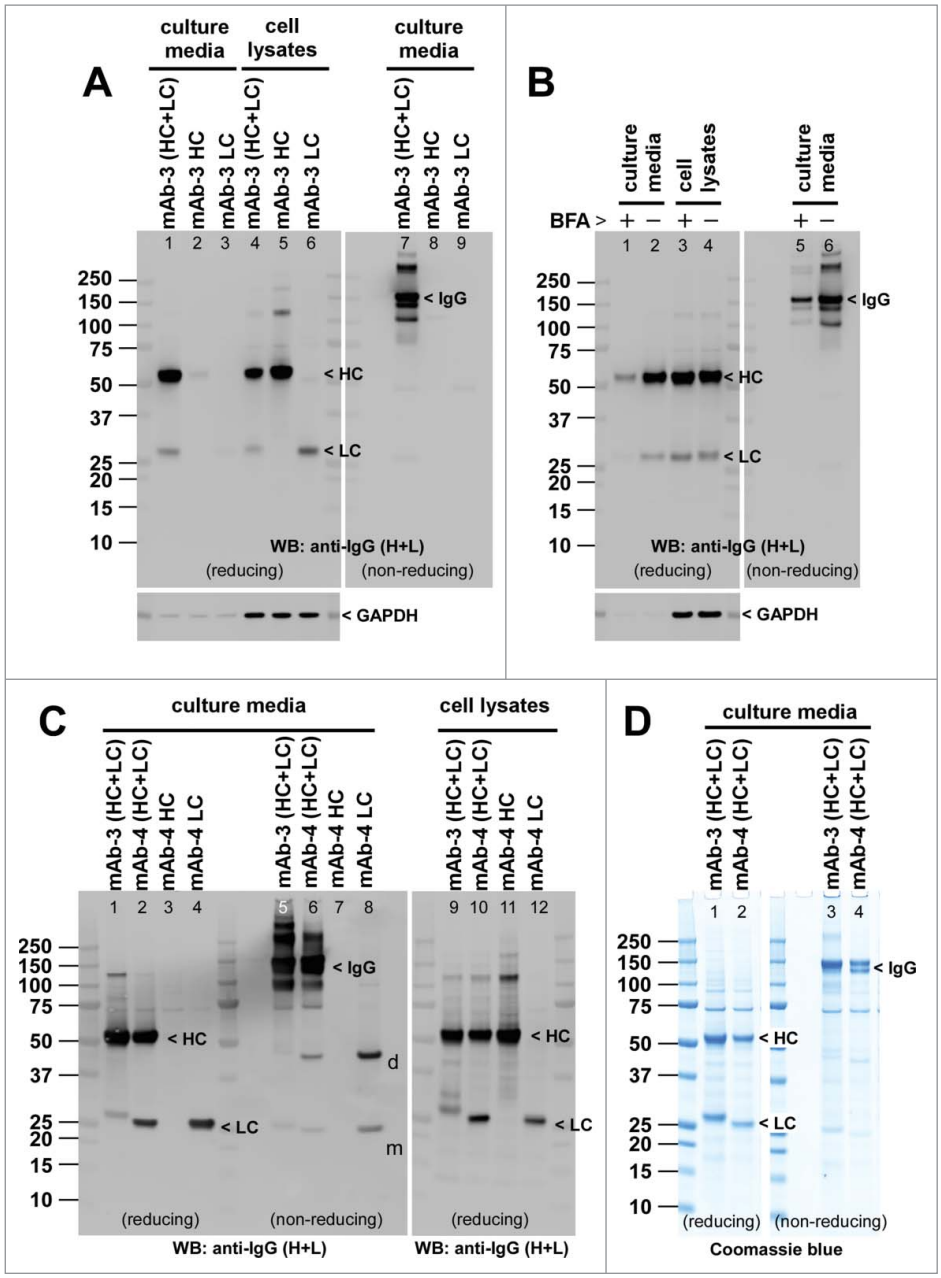

Figure 2. Model mAb-3 is secretion competent. (A) Cell culture media and whole cell lysate samples were prepared on day-7 post transfection and were subjected to SDS-PAGE followed by Western blot using rabbit anti-human IgG (H + L) polysera. Harvested cell culture medium was loaded and analyzed under reducing conditions (lanes 1–3) or non-reducing conditions (lanes 7–9). Whole cell lysates were loaded under reducing conditions (lanes 4–6). Expected band for heavy chain (HC), light chain (LC), or the whole IgG is marked by arrowhead and labeled accordingly. Anti-GAPDH blot is shown at the bottom as a loading reference. Both γ2-HC (lanes 2, 8) and λ-LC (lanes 3, 9) were secretion incompetent by themselves. The used constructs are shown at the top of corresponding lanes. (B) On day-2 post transfection, cell culture media were replaced with fresh growth media with or without 15 μg/ml BFA and maintained in suspension format for 24 hr until day-3 when the cell culture media and cell pellets were harvested and analyzed. The amount of mAb-3 protein secreted to the culture medium during the 24 hr BFA treatment is in lanes 1–2 (reducing conditions) and lanes 5–6 (non-reducing conditions). The amount of IgGs detected in the cell lysates is shown in lanes 3–4 (reducing conditions). Anti-GAPDH blot is shown as a loading reference for cell lysate samples. (C) Expression analysis of mAb-4. Cell culture media and whole cell lysate samples were prepared on day-7 post transfection and were analyzed as above. Expected band for HC, LC, or whole IgG is marked by arrowhead and labeled. (D) Expression comparison of mAb-3 and mAb-4. Cell culture media were harvested from mAb-3 and mAb-4 transfected cells on day-7 post transfection and analyzed under reducing (lanes 1, 2) or non-reducing (lanes 3, 4) conditions. SDS-PAGE gel was stained by Coomassie blue.

CBs co-localized with ER markers such as ERp57 and BiP (Fig. 4 BC). This co-localization supported that CBs were housed in the membranes of ER origin. Co-localization with the ER resident proteins also demonstrated that this crystal-storing phenotype was distinct from pseudo-Gaucher cell phenotypes where Ig crystals were deposited in lysosomes.[15]

Because this γ2-HC subunit came from mAb-1 that readily induced rod-shaped CBs in the ER,[17] we suspected at first that this γ2-HC subunit might induce crystalline inclusions when paired with any LCs. To address this concern we co-expressed the γ2-HC subunit of mAb-1/mAb-3 with an unrelated isotype-matched λ-LC subunit (denoted as lambda-LC* in Fig. 5A). Both under steady-state growth condition and BFA treatment, this *ad hoc* control mAb failed to induce CBs (Fig. 5A). Likewise, when the model λ-LC of mAb-2/mAb-3 was co-expressed with its cognate mAb-2 γ2-HC (denoted as

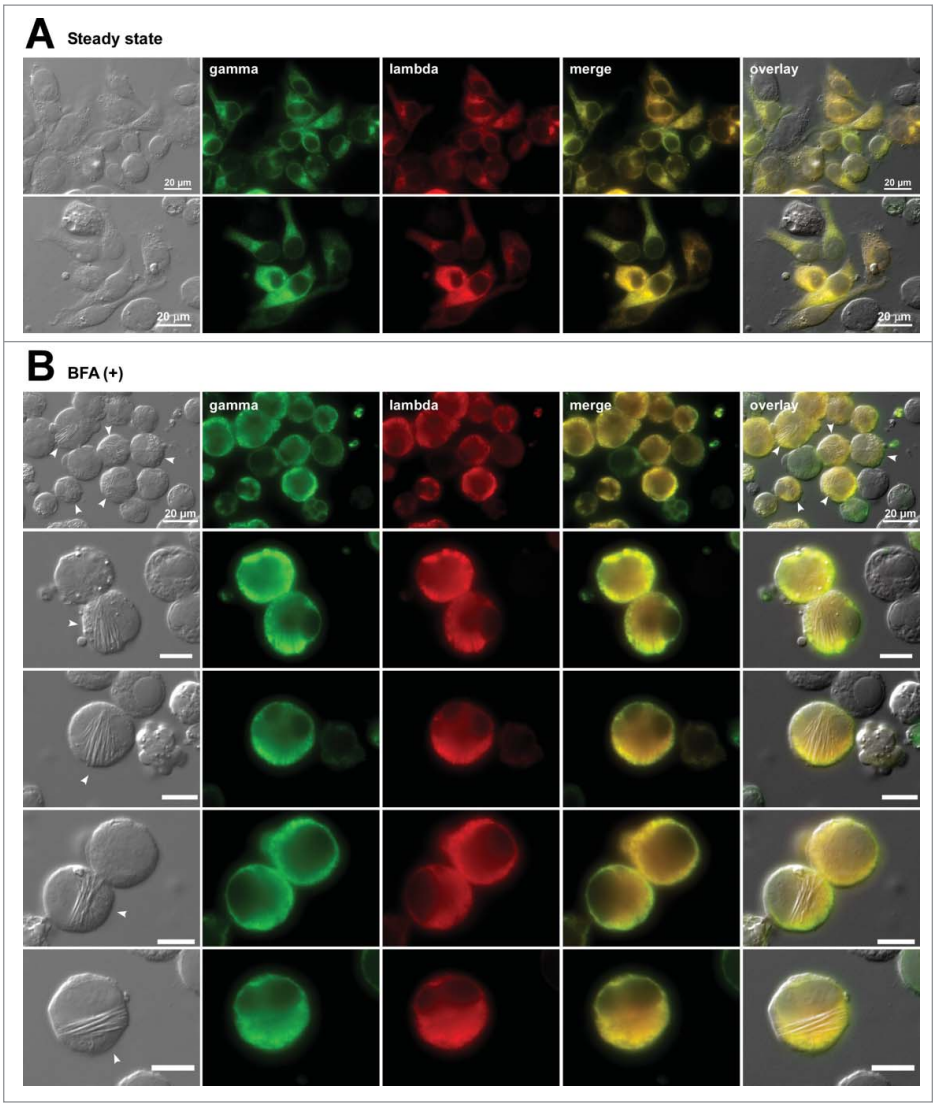

Figure 3. The mAb-3 expressing cells induce needle-like crystalline inclusion bodies when ER-to-Golgi transport is blocked. Fluorescent micrographs of HEK293 cells transfected to express mAb-3. On day-2 post transfection, HEK293 cells were resuspended in fresh cell culture media with or without 15 μg/ml BFA, then immediately seeded onto poly-lysine coated glass coverslips and statically cultured for 24 hr. On day-3, cells were fixed, permeabilized, and immuno-stained. Co-staining was performed by using FITC-conjugated anti-gamma chain and Texas Red-conjugated anti-lambda chain polyclonal antibodies. Green and red image fields were superimposed to create 'merge' views. DIC and 'merge' were superimposed to generate 'overlay' views. (A) Subcellular localization of gamma-chain and lambda-chain in co-transfected cells was visualized under steady-state normal cell growth conditions. Two representative image fields are shown. (B) Gamma- and lambda-chains of the mAb-3 were visualized after 24 hr BFA treatment. Five representative image fields are shown. Crystal-laden cells are pointed by arrowheads in DIC images. The CB phenotype frequency after the BFA treatment is stated in the text. Unlabeled scale bar represents 10 μm.

gamma2-HC* in Fig. 5B), the resulting mAb-2 also failed to induce CBs both at steady-state and under BFA treatment (Fig. 5B). Therefore, the acidic surface patch composed of eight Asp residues (five from CDR-H3 and three from CDR-L2) was required for this needle-like crystallization event.

Individual subunit chains of mAb-3 are not able to induce crystalline inclusion bodies when expressed alone.

There are at least two reported cases where the LC subunit alone was sufficient to induce intracellular CBs. The first case was a human λ-LC expressed in bone marrow derived B lymphocytes from chronic lymphocytic leukemia patient,[22] and the second was a murine hybridoma clone F10 expressing a κ-LC.[23] To our knowledge there are no reported instances of CB induction by the HC subunit alone.

To examine the crystallizing propensity, if any, of the individual subunits comprising the model mAb-3, we expressed each subunit chain individually and examined the transfected cells by microscopy for the presence of notable cell phenotypes. The LC-only expressing cells exhibited morular cell phenotype in which the cells were filled with numerous spherules (Fig. 6A). Immunofluorescent imaging indicated that those spherules were composed of the LC proteins. Similarly, the HC subunit of this model mAb also induced similar morular cell phenotype (Fig. 6B). These spherule formations are the hallmark characteristics of protein condensation via liquid-liquid phase separation in the ER.[24] Of note, morular cell phenotypes are alternatively referred to as grape cells.[25] Because both subunit chains were secretion incompetent to begin with, we did not evaluate the effects of BFA on cell phenotypes. The morphological evidence presented here suggested that individual

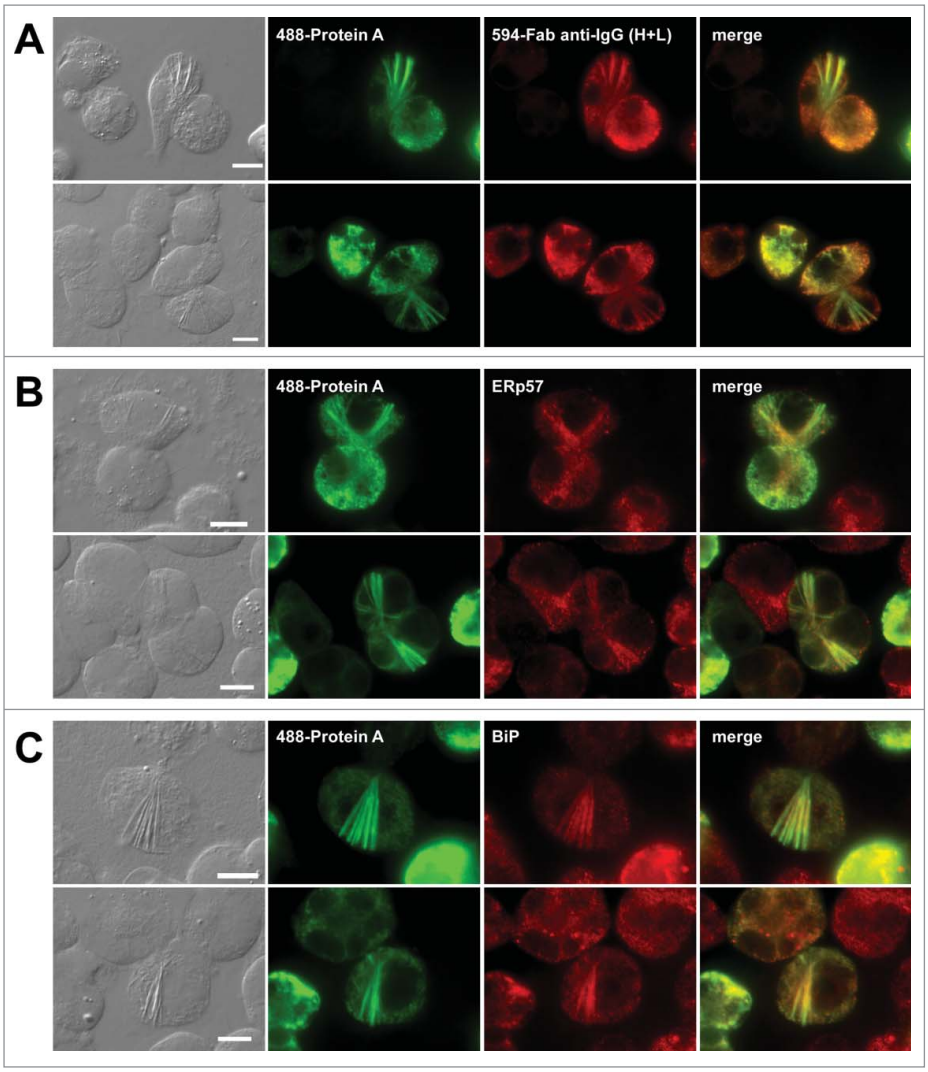

Figure 4. Needle-like crystalline inclusions co-localize with ER resident proteins. Fluorescent micrographs of HEK293 cells transfected to express mAb-3. On day-2 post transfection, HEK293 cells were resuspended in fresh cell culture media containing 15 μg/ml BFA, then immediately seeded onto poly-lysine coated glass coverslips and statically cultured for 24 hr. On day-3, cells were fixed, permeabilized, and immuno-stained. (A) Co-staining was performed by using Alexa Fluor 488-conjugated Protein A and Alexa Fluor 594-conjugated Fab fragments generated from goat anti-human IgG (H + L) polysera. (B, C) Transfected cells were co-stained with Alexa Fluor 488-conjugated Protein A and anti-ERp57 (B) or anti-BiP (C). Green and red image fields were superimposed to create 'merge' views. Scale bars represent 10 μm.

subunit chains had intrinsically high condensation propensity and therefore phase-separated into numerous spherical droplets in the ER when the partner subunit was missing. These observations led us to conclude that the crystallizing propensity was separately embedded in individual subunits, but it was generated *de novo* only when the two subunit chains assembled into a whole IgG molecule.

The negatively-charged surface patch on the variable domain was not sufficient for crystalline inclusion formation.

If the acidic patch on the variable domain surface is sufficient to impart mAb-3 the crystallizing propensity, a subtype switched version of mAb-3 would be equally prone to produce crystalline inclusions in the ER. To test this possibility, we made a mAb-3 HC construct with the γ1 subtype and co-expressed it with the mAb-3 λ-LC. Firstly, changing the subtype to IgG1 did not have a major effect on mAb secretion (232.7 $\pm$ 25.4 mg/L, n = 4; Fig. 7 AB, lanes 1, 2, 11, 12). Secondly, the γ1-HC subunit was secretion incompetent by itself as expected (Fig. 7 AB, lanes 4, 5, 9, 10, 14, 15). Thirdly, both at steady-state and under BFA treatment, the IgG1 version of the mAb-3 failed to induce CBs (Fig. 7C, D). Lastly, instead of inducing the characteristic morular cell phenotypes, the γ1-HC by itself distributed to the ER and Golgi, and did not produce notable cell phenotypes (Fig. 7E). These results demonstrated that crystallizing propensity emerged selectively when the HC subunit was of the γ2 subtype. Therefore, the acidic surface patch on the variable domain alone was not sufficient to trigger this crystallization event.

The intact acidic patch is necessary for high-level secretion and intracellular crystallization of mAb-3.

The results obtained above implicated that intermolecular interactions between the variable domain acidic patch and the IgG2 constant domain underscored this needle-like crystalline formation. To examine the underlying intermolecular interactions between these two separate elements from a different

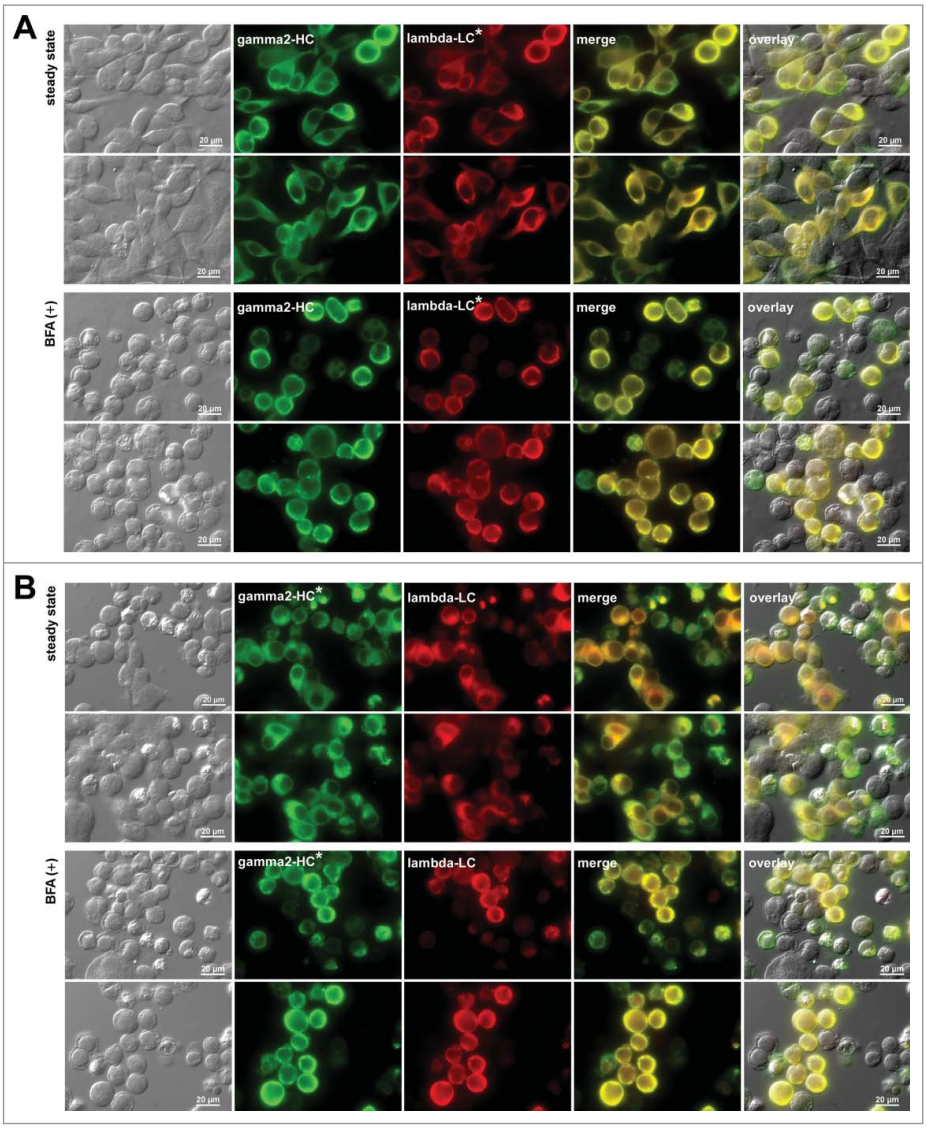

Figure 5. Crystalline inclusion bodies are not induced if γ2-HC or λ-LC of mAb-3 is replaced by an isotype-matched subunit chain. Fluorescent micrographs of HEK293 cells transfected with (A) mAb-3 γ2-HC and unrelated isotype-matched λ-LC (denoted as lambda-LC*) and (B) mAb-3 λ-LC and mAb-2 γ2-HC (denoted as gamma2-HC*). On day-2 post transfection, HEK293 cells were resuspended in fresh cell culture media with or without 15 μg/ml BFA, then immediately seeded onto poly-lysine coated glass coverslips and statically cultured for 24 hr. On day-3, cells were fixed, permeabilized, and immuno-stained. Co-staining was performed by using FITC-conjugated anti-gamma chain and Texas Red-conjugated anti-lambda chain polyclonal antibodies. In panels A and B, first two rows are the representative image fields under steady-state growth conditions, whereas rows three and four are under BFA treatment. Green and red image fields were superimposed to create 'merge' views. DIC and 'merge' were superimposed to generate 'overlay' views.

perspective, we substituted the five Asp residues in CDR-H3 with Ala and/or the three Asp residues in CDR-L2 with Ala, then examined the effects of stepwise Asp-to-Ala substitution on secretion output and CB phenotype occurrence. When five Asp residues of the CDR-H3 were mutated to Ala, the secretion level dropped 45% to 154.8 $\pm$ 15.6 mg/L (n = 4) (Fig. 8 AB, lanes 1–2) compared to the parental mAb-3. Similarly, when three Asp residues in CDR-L2 were substituted with Ala, the secretion of the mutant mAb fell 60% to 109.3 $\pm$ 14.6 mg/L (n = 4) (Fig. 8 AB, lanes 1 and 3). Lastly, when all eight Asp residues were mutated to Ala simultaneously, the secretion titer fell 76% to 64.5 $\pm$ 12.6 mg/L (n = 4) (Fig. 8 AB, lanes 1 and 4).

Regardless of the Asp-to-Ala substitution, the HC and LC subunits remained secretion incompetent by themselves (Fig. 8 A–C, lanes 5–8). Interestingly, Asp-to-Ala substitution in CDR-H3 increased the aggregation propensity of the HC subunit as evidenced by the appearance of high molecular weight species even in the presence of SDS and β-mercaptoethanol (Fig. 8C, lane 5). The secretion titer difference observed in Asp-to-Ala mutants unexpectedly uncovered an additional role of the acidic surface patch in maintaining mAb-3's high-level secretion outputs, perhaps by modulating the solubility of mAb-3.

When it comes to the steady-state subcellular distribution of mAbs, both HC and LC subunits localized broadly in the ER and Golgi in the cells expressing parental mAb-3 (Fig. 9A) and the cells expressing mutant mAb-3 in which either HC or LC was mutated (Fig. 9 BC). When all eight Asp residues were simultaneously mutated to Ala, there was an acute increase in the induction of Russell body (RB) phenotypes[21,26,27] (Fig. 9D, ~35%; 77 RB-positive cells/219 transfected cells). Furthermore, while Asp-to-Ala mutated LC alone induced morular cell phenotype (Fig. 6C), Asp-to-Ala mutated HC now predominantly

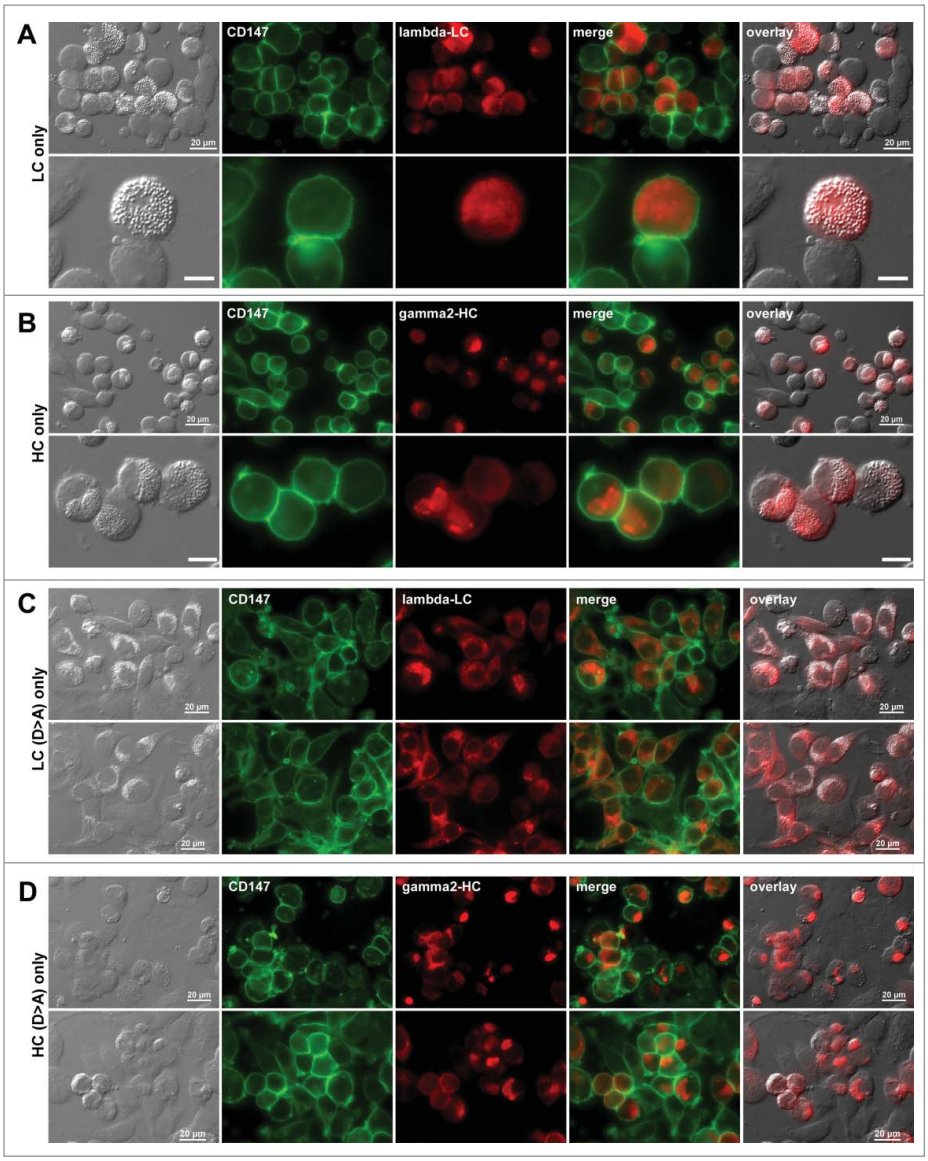

Figure 6. Individual subunit chains of mAb-3 do not induce crystalline inclusion bodies. Fluorescent micrographs of HEK293 cells transfected with (A) mAb-3 λ-LC construct alone, (B) mAb-3 γ2-HC construct alone, (C) Asp-to-Ala mutated mAb-3 λ-LC alone, and (D) Asp-to-Ala mutated mAb-3 γ2-HC alone. On day-2 post transfection, suspension cultured cells were seeded onto poly-lysine coated glass coverslips and statically cultured for 24 hr. On day-3, cells were fixed, permeabilized, and co-stained with anti-CD147 and anti-lambda chain (A and C). In panels B and D, cells were co-stained with anti-CD147 and anti-gamma chain. Endogenous CD147 was stained to highlight cell shapes. Green and red image fields were superimposed to create 'merge' views. DIC and 'red' were superimposed to generate 'overlay' views. Unlabeled scale bar represents 10 μm.

induced RB phenotypes (Fig. 6D). This notable phenotype alteration reflected the changes in the condensation propensity of HC subunit due to charge neutralization. These observations were in good agreement with our previous findings showing the correlation between the poor IgG secretion and the high occurrence of RB phenotype.[21,27]

BFA treatment induced the characteristic needle-like inclusion bodies in the cells expressing the parental mAb-3 as before (Fig. 10A, arrowheads). If one of the subunits was replaced by the Asp-to-Ala version, resulting mAb-3 mutants no longer induced CBs (Fig. 10 BC). When both subunit chains were simultaneously replaced by the Asp-to-Ala mutant subunits, the mAb induced the RB phenotypes more extensively (Fig. 10D, ~56%; 181 RB-positive cells/322 transfected cells). The results clearly demonstrated the requirement of the intact acidic surface patch in needle-like CB formation in the IgG2 subtype context. The experiments in this section solidified that amino acid substitutions that hamper intermolecular interactions between the variable domain acidic patch and the γ2-HC constant domain abolished needle-like crystalline inclusion formation in the ER.

Discussion

Despite the abundant clinical and pathological case reports on intracellular Ig crystals in plasma cells, there have been very few studies that addressed the underlying processes of intracellular Ig crystallization events. In this study, we elucidated one such mode of an intra-ER Ig crystallization event using a human mAb that possessed a prominent negatively-charged surface cluster on the variable domain. The identified crystallization process required the interactions between the acidic patch on the variable domain and still undefined elements on γ2-HC constant domain, and these interactions served as the biochemical basis for multivalent interactions leading to the

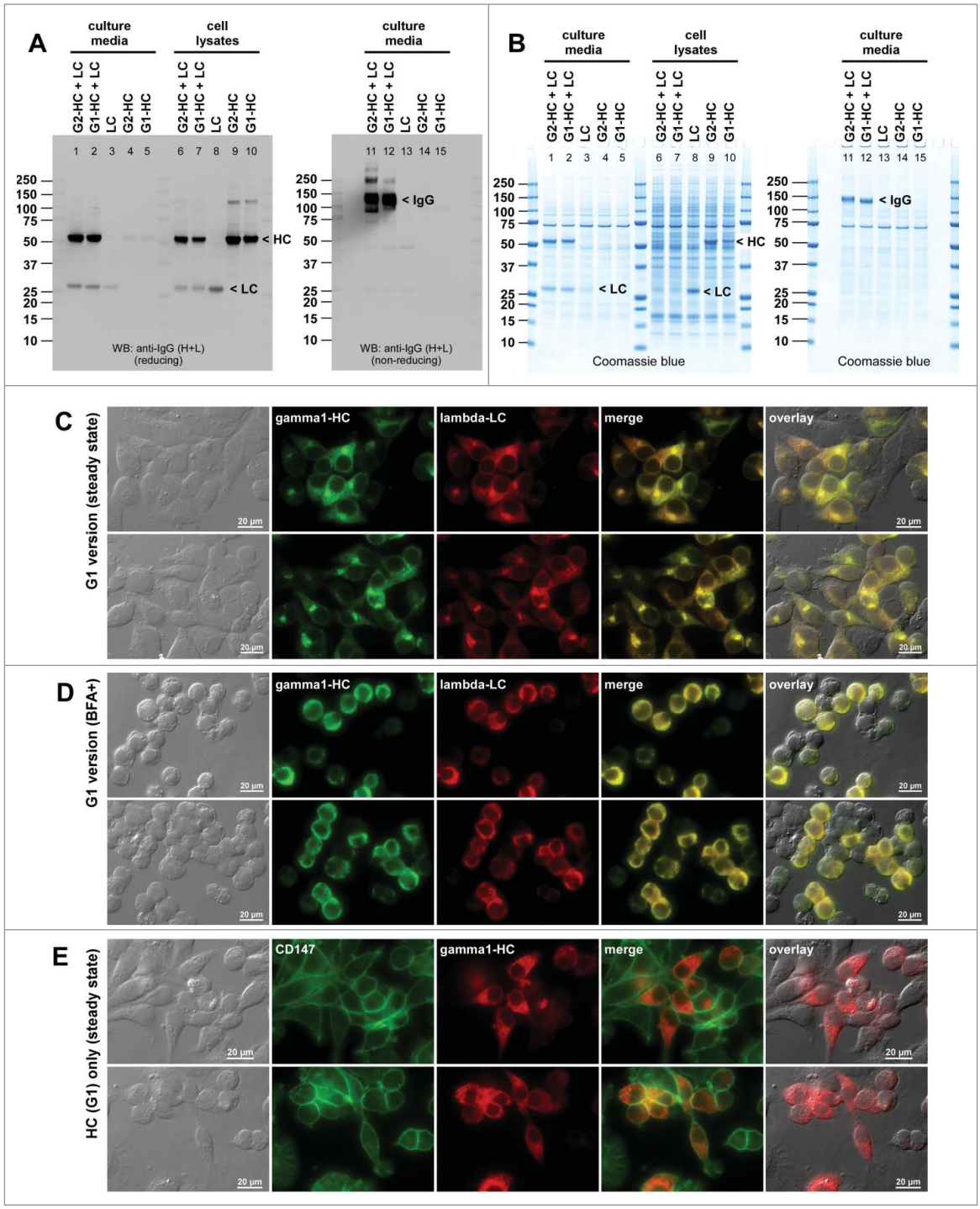

Figure 7. IgG1 version of mAb-3 does not induce crystalline inclusion bodies. (A) Cell culture media were harvested on day-7 post transfection and were subjected to SDS-PAGE under reducing conditions (lanes 1–5) or non-reducing conditions (lanes 11–15). Cell lysates were analyzed under reducing conditions (lanes 6–10). Western blotting was performed using anti-human IgG (H + L) polysera. Constructs used are shown at the top of corresponding lanes. Expected band for HC, LC, or the whole IgG is marked by arrowhead and labeled. (B) The same set of samples analyzed in panel A were stained by Coomassie blue dye. (C, D) Fluorescent micrographs of HEK293 cells expressing the IgG1 version of mAb-3. On day-2 post transfection, HEK293 cells were resuspended in fresh cell culture media with or without 15 μg/ml BFA, then seeded onto poly-lysine coated glass coverslips and statically cultured for 24 hr. On day-3, cells were fixed, permeabilized, and immuno-stained. Co-staining was performed by using FITC-conjugated anti-gamma chain and Texas Red-conjugated anti-lambda chain polyclonal antibodies. Green and red image fields were superimposed to create 'merge' views. DIC and 'merge' were superimposed to generate 'overlay' views. (E) Fluorescent micrographs of HEK293 cells transfected with the γ1 version of mAb-3 HC construct alone. On day-3, cells were fixed, permeabilized, and co-stained with anti-CD147 and anti-gamma chain. Green and red image fields were superimposed to create 'merge' views. DIC and 'red' were superimposed to generate 'overlay' views.

formation of needle-like CBs in the ER. The details of actual contacting interfaces and the underlying amino acid side chain interactions await successful X-ray crystallographic studies using the cell-derived crystals either *in situ* or after isolating them from the cells. Whether we can technically isolate and preserve these thin needles outside of the cells and whether these needle-like crystalline bodies are of diffraction quality for X-ray crystallography need to be investigated further.

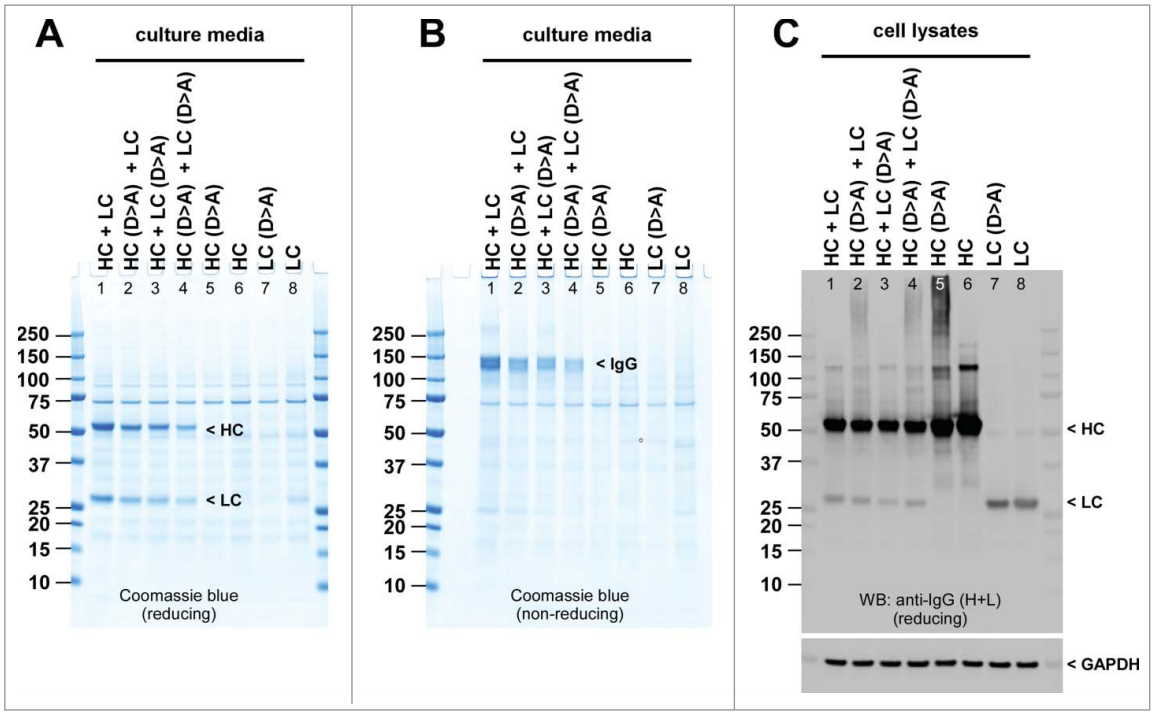

Figure 8. Stepwise neutralization of acidic surface patch progressively diminishes mAb-3 secretion. HEK293 cells were co-transfected with the parental subunits or the Asp-to-Ala mutated subunits in various combination. Cell culture media were harvested on day-7 post transfection and were analyzed by SDS-PAGE under reducing (A) or non-reducing (B) conditions followed by Coomassie blue staining. Whole cell lysates were loaded under reducing conditions (C) followed by Western blotting using anti-human IgG (H + L) polysera. Expected band for HC, LC, or the whole IgG is marked by arrowhead and labeled. Anti-GAPDH blot is shown as a loading reference for cell lysate samples.

While intrinsic properties embedded in the mAb-3 itself (i.e., intact acidic patch and γ2-HC subtype) were required to trigger a crystallization event in the ER, they were not sufficient. As shown previously for a different set of crystallizing human IgGs,[17,18] the concentration of assembled mAb-3 needed to surpass a certain threshold concentration in the ER lumen before crystallization could take place, perhaps via a rate-limiting nucleation step. In the employed HEK293 transient expression system a pharmacological blockade of ER-to-Golgi transport helped mAb-3 proteins reach such concentration. Determining the actual threshold concentration using purified protein components was not attempted in this study because it would require a precise reconstitution of physiological ER environment in test tubes.

Do all mAbs come to induce CBs in the ER if they possess a prominent acidic surface patch on the variable domain? The answer to this question seems to be "No." Even though mAb-2 was predicted to possess an acidic surface patch composed of three Asp residues in CDR-L2 (unpublished data), this antibody did not induce CBs under the same transfection and cell culture conditions (see Fig. 5B). Likewise, the control mAb shown in Fig. 5A also failed to induce CBs during overexpression despite it having an acidic surface patch composed of five Asp residues. Evidently, there are still unknown physicochemical requirements in addition to just having a prominent acidic patch in order to predispose the mAbs for CB formation. In an attempt to find a potential relationship between the isoelectric point of mAbs and the likelihood of CB formation, we summarized relevant information in Table-1. By looking at those values, it seems difficult to find correlations among the CB-inducing propensity, the isoelectric point of mAbs, and the neutral pH of the ER lumen[28].

Influence of localized surface charge cluster on the solution behaviors of purified IgGs have attracted attention in biopharmaceutical formulation development. Accrued evidence showed that localized charge clusters promoted self-association of purified mAbs at high protein concentration, thereby resulting in undesirably high solution viscosity or peculiar phase behavior.[29,30] Similar to the settings of biopharmaceutical formulation in glass vials, the ER lumen is a highly crowded environment because of the overexpressed secretory proteins and the ER resident proteins that inevitably interact each other during protein biosynthesis. For instance, in Hela cells, the concentration of ER-resident protein BiP alone was estimated to reach 90 to 120 mg/ml in the ER after recombinant expression of a mouse Ig μ-HC, while the total protein concentration in the ER in the same cell can reach 200 to 300 mg/ml.[31] Whether the mAbs that display undesirable solution behaviors *in vitro* would also induce noticeable cell phenotypes during mAb overexpression is an important topic that needs to be addressed further.

There is one example of a human IgG2λ clone that induced grain-shaped CBs without revealing notable charge clusters on the surface of its variable domain.[18] For this particular IgG2λ mAb, switching the HC subclass from γ2 to γ1 or γ4 changed the CB morphology drastically, while switching to γ3 abrogated crystallization.[18] Evidently, different types of intermolecular interactions other than something which relies on an acidic surface patch appear to govern the intra-ER crystallization event of this human IgG2λ mAb. There is little doubt that different mAbs call for different modes of intermolecular interactions and threshold concentrations before crystallization ensues in the ER lumen. Whether such conditions can be met under physiological or abnormal cell growth conditions is an important factor that

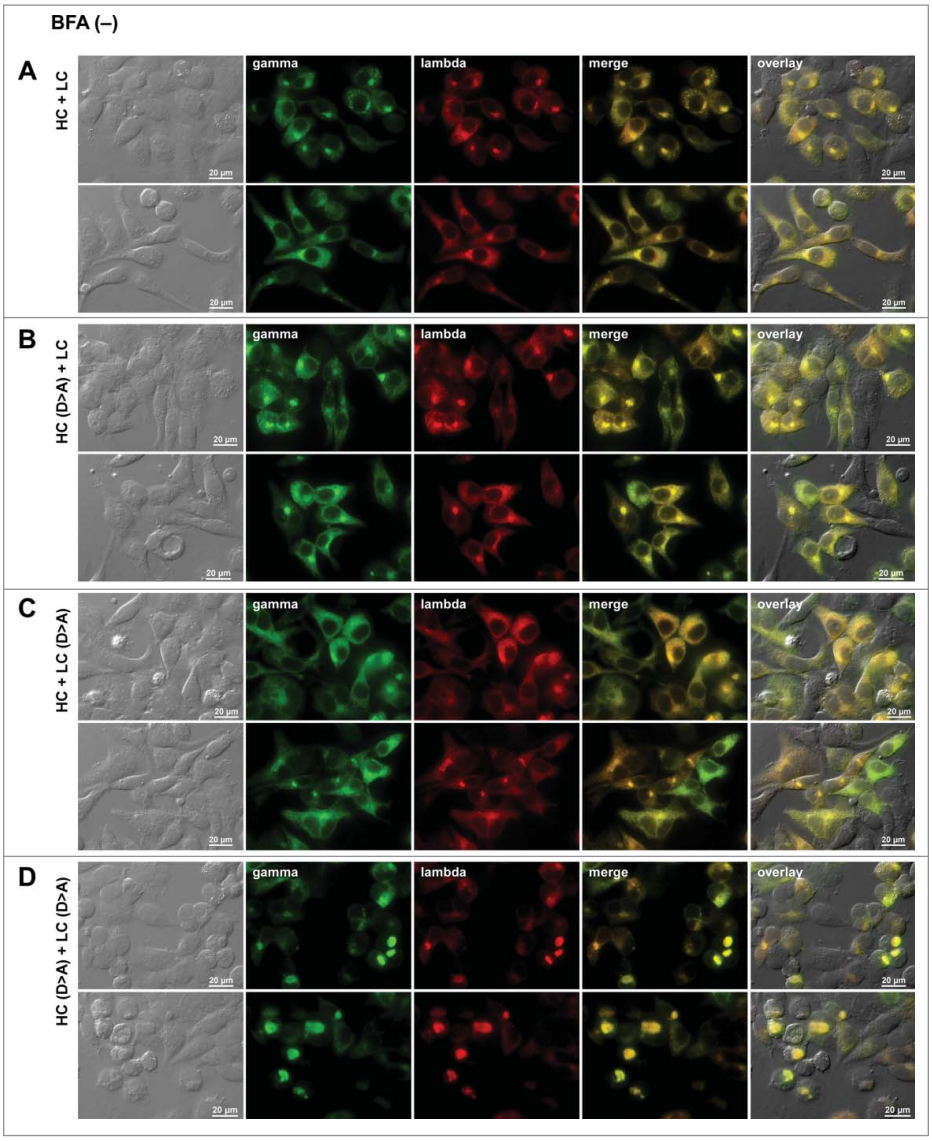

Figure 9. Neutralization of acidic patch leads to Russell body induction. Fluorescent micrographs of HEK293 cells transfected with the following construct(s): (A) the parental HC and LC subunits; (B) Asp-to-Ala mutated version of HC and the parental LC; (C) the parental HC and Asp-to-Ala mutated version of LC; (D) Asp-to-Ala mutated versions of HC and LC subunits. On day-2 post transfection, suspension cultured cells were seeded onto poly-lysine coated glass coverslips and statically cultured for 24 hr. On day-3, cells were fixed, permeabilized, and immunostained. Co-staining was carried out with FITC-conjugated anti-gamma chain and Texas Red-conjugated anti-lambda chain polyclonal antibodies. Green and red image fields were superimposed to create 'merge' views. DIC and 'merge' were superimposed to generate 'overlay' views.

dictates the prevalence of intracellular Ig crystallization events. Genetic or epigenetic changes that are to occur in the transformed plasma cells may play additional roles in promoting the occurrence of Ig crystallization in plasma cell dyscrasias by modulating the biosynthetic capacity of afflicted cells.

Materials and methods

Detection antibodies and reagents

Mouse monoclonal anti-GAPDH (cat. MAB374) was obtained from Chemicon. Mouse monoclonal anti-CD147 (cat. 555961) was from BD Biosciences. Affinity purified rabbit polyclonal anti-human IgG (H + L) polysera (cat. 309-005-082) used for Western blotting and Alexa Fluor® 594-conjugatged Fab fragment goat anti-human IgG (H + L) (cat. 109-587-003) used for imaging were from Jackson ImmunoResearch Laboratories. FITC- or Texas Red-conjugated goat polyclonal anti-human gamma-chain (cat. 2040-02, cat. 2040-07) and anti-human lambda-chain (cat. 2070-02, cat. 2070-07) were from Southern Biotech. Alexa Fluor® 488-conjugated Protein A (cat. P11047), Alexa Fluor®-488, -594, and -680 conjugated goat polyclonal anti-mouse IgG (H + L) and rabbit IgG (H + L) antibodies were purchased from Thermo Fisher Scientific. All the chemicals and biological reagents were obtained from Sigma-Aldrich unless specifically mentioned.

Expression constructs

Coding sequences for both LC and HC subunits of the human mAb-1[17] and mAb-2 [19] (see Fig. 1A, top) were obtained from hybridoma cell lines derived from immunized Xenomouse™ by using the molecular cloning method described previously.[21] The nucleotide sequences encoding LC and HC subunits were individually subcloned into pTT5 expression vectors (licensed

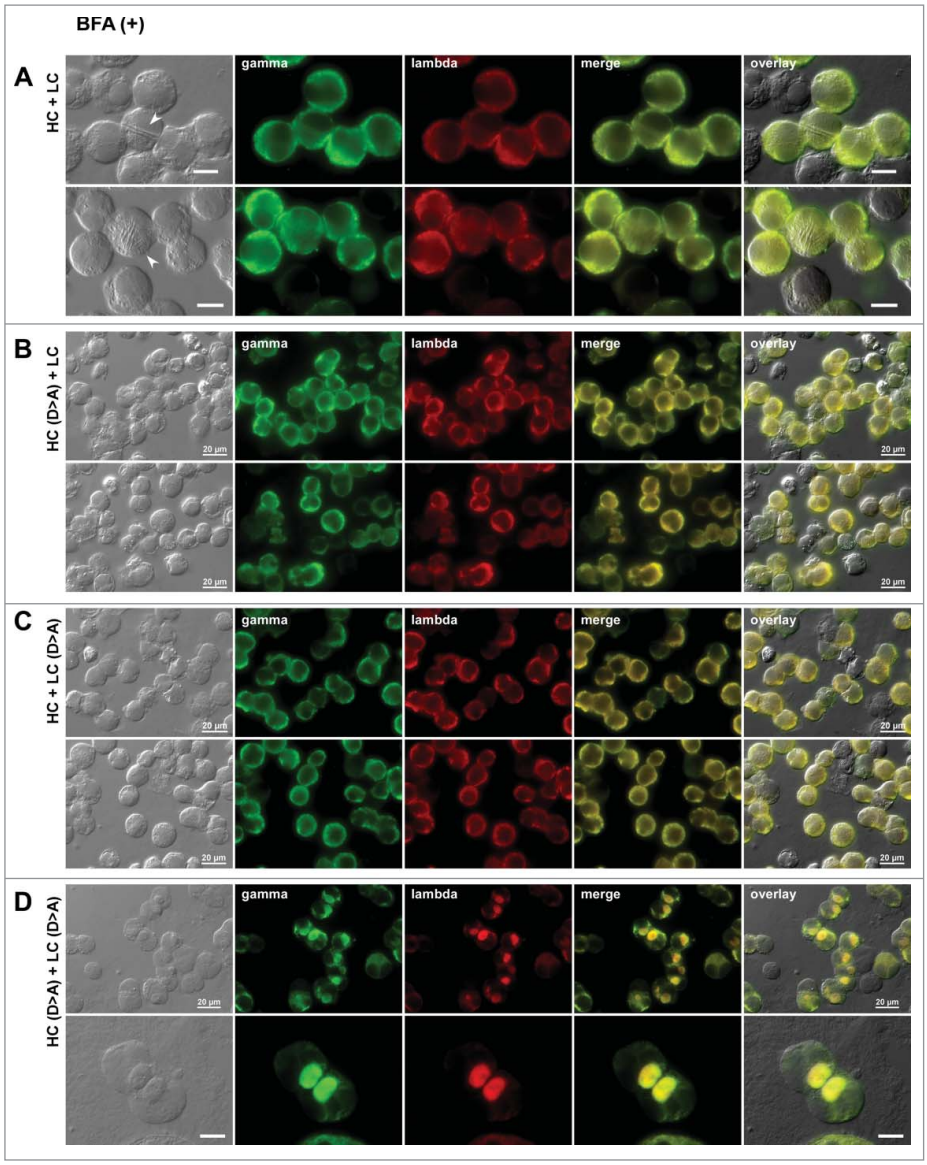

Figure 10. Loss of acidic surface patch promotes Russell body induction under ER-to-Golgi transport block. Fluorescent micrographs of HEK293 cells transfected with the following construct(s): (A) the parental HC and LC subunits; (B) Asp-to-Ala mutated version of HC and the parental LC; (C) the parental HC and Asp-to-Ala mutated version of LC; (D) Asp-to-Ala mutated versions of HC and LC subunits. On day-2 post transfection, HEK293 cells were resuspended in fresh cell culture media containing 15 μg/ml BFA, then seeded onto poly-lysine coated glass coverslips and statically cultured for 24 hr. On day-3, cells were fixed, permeabilized, and co-stained with FITC-conjugated anti-gamma chain and Texas Red-conjugated anti-lambda chain polyclonal antibodies. Green and red image fields were superimposed to create 'merge' views. DIC and 'merge' were superimposed to generate 'overlay' views. Crystal-laden cells are pointed by arrowheads in panel A. Unlabeled scale bar, 10 μm.

from National Research Council of Canada) by a set of commonly used molecular cloning techniques. Site-directed Asp-to-Ala amino acid substitutions were carried out by using widely used PCR-based mutagenesis techniques.

Cell culture, transient transfection, and protein production method

HEK293-EBNA1(6E) cells (hereafter HEK293 cells) were licensed from National Research Council of Canada for research use. HEK293 cells were cultured in a humidified Reach-In CO_2 incubator (37 °C, 5% CO_2) using FreeStyle™ 293 Expression Medium (Thermo Fisher Scientific). HEK293 cells were maintained in suspension culture format in Corning® Erlenmeyer cell culture flasks placed on an Innova 2100 shaker platform (New Brunswick Scientific) rotating at 110 rpm. Expression constructs were transfected into HEK293 cells using the protocol described in detail previously.[21] To express and produce whole IgG mAb, a designated pair of HC and LC constructs were co-transfected at the plasmid DNA ratio of one-to-one (normalized by mass). When individual subunit chains were expressed separately, 50% of the total DNA was substituted with an empty pTT5 vector to normalize gene dosage. Difco yeastolate cell culture supplement (BD Biosciences) was added to the cell culture at 24 hr post transfection. Cell culture media were harvested and the whole cell lysates were prepared on day-7 post transfection for various analytical purposes including IgG titer determination and Western blotting. Concentration of human IgG in the harvested cell culture media was determined by bio-layer interferometry with an Octet RED96 (ForteBio) using Protein A biosensor probes in 96-well microtiter plates.

Immunofluorescent microscopy

To carry out fluorescent cell imaging at steady-state or under ER-to-Golgi transport block conditions, growth media of suspension cultured HEK293 cells were replaced with fresh media without or with 15 μg/ml brefeldin A (BFA) at 48 hr post transfection. Immediately after the media replacement, one million cells were withdrawn from each shake flask and seeded onto poly-L-lysine coated glass coverslips placed in 6-well plates. After 24 hr of static cell culture, cells were fixed in 0.1 M sodium phosphate buffer (pH 7.2) containing 4% paraformaldehyde for 30 min at room temperature. After washing steps in PBS containing 0.1 M glycine, fixed cells were soaked in permeabilization buffer (PBS containing 0.4% saponin, 1% BSA, 5% fish gelatin) for 15 min, followed by an incubation with primary antibody diluted in the permeabilization buffer for 60 min. After three washes in permeabilization buffer, the cells were stained with secondary antibodies for 60 min in permeabilization buffer. Coverslips were mounted onto slide-glass using Vectashield mounting media (Vector Laboratories) and cured overnight at 4 °C in the dark. The slides were analyzed on Nikon Eclipse 80i microscope with a 100 × or 60 × CFI Plan Apochromatic oil objective lens and Chroma FITC-HYQ or Texas Red-HYQ filter. Images were acquired using a Cool SNAP HQ2 CCD camera (Photometrics) and Nikon Elements imaging software. To determine the prevalence of crystalline inclusion bodies and Russell bodies in a population of transfected cells, microscopic images of 10–30 fields were captured for each construct set using 60 × objective lens. Based on the anti-gamma and/or anti-lambda staining, the total number of transfected cells was first determined. The number of designated phenotype-positive cells was then determined by visually inspecting individual images.

SDS-PAGE and Western blotting

On day-7 post transfection, aliquots of suspension cell culture were withdrawn from shake flasks, and the culture media were separated from cell pellets by centrifugation at 1000 g for 5 min. Harvested cell culture media were mixed with 2 × SDS-containing denaturing sample buffer (Thermo Fisher Scientific). Cell pellets were directly lysed in 1 × sample buffer. Both samples were heated at 75 °C for 5 min. To prepare protein samples under reducing conditions, β-mercaptoethanol was included in the sample buffer to a final concentration of 5% (v/v). To prepare samples under non-reducing conditions, the reducing agent was omitted, but 2 mM N-ethylmaleimide was included as an alkylating agent to quench reactive free cysteine residues. To normalize sample loading, whole cell lysates corresponding to 12,000-12,500 cells were analyzed per lane. To compare the differences in volumetric secretion titers, a sample volume equivalent to 5 μl of harvested culture medium was analyzed per lane. SDS-PAGE was performed using NuPAGE 4–12% Bis-Tris gradient gel and a compatible MES SDS buffer system (both from Thermo Fisher Scientific). Resolved proteins were electrotransferred to a nitrocellulose membrane, blocked, and probed with primary antibodies of choice. After three washes in PBS containing 0.05% (v/v) Tween-20, the nitrocellulose membranes were probed with Alexa Fluor 680-conjugated secondary antibodies (Thermo Fisher Scientific). After three rounds of washing, the membranes were scanned to acquire Western blotting data using Odyssey® infrared imaging system (LI-COR Biosciences).

Structural modeling of IgG variable fragment (Fv)

Homology models of mAb-3 were generated by the method described previously.[17] In brief, a suitable Fv template was selected using the Antibody Modeling module in Molecular Operating Environment (MOE; Chemical Computing Group, Montreal, Canada), which considers structural resolution and B-factors of the template structure in addition to identity to query sequence. The individual CDRs were then used to search the PDB[32] to find CDR structure templates from all known antibody structures that match in length to the query CDRs. The best template was selected based on highest identity to the query CDR, structural resolution, and B-factors of the templates. The chosen template CDRs were placed onto the chosen Fv framework by superposition of the Cα carbons from the three residues on either side of each CDR. The final homology model was built from this template using MOE.

Abbreviations

CB	crystalline body
CDR	complementarity-determining region
CHO	Chinese hamster ovary
DIC	differential interference contrast
ER	endoplasmic reticulum
Fab	antigen binding fragment
Fc	crystallizable fragment
Fv	variable fragment
HC	heavy chain
HEK	human embryonic kidney
Ig	immunoglobulin
LC	light chain
mAb	monoclonal antibody
RB	Russell body

Disclosure of potential conflicts of interest

No potential conflicts of interest were disclosed.

Acknowledgments

The authors thank Allison Bianchi and Jane Carter for making mAb-2 expression constructs and Ai Ching Lim for critically reviewing the manuscript.

Author contributions

Study conception and design: HH
Critical reagent generation: LL, KG, FJ
Acquisition of data: HH, MG, RRK
Analysis and interpretation of data: HH
Drafting of manuscript: HH
Critical revision: HH, RRK, FJ
Final approval of manuscript: HH, MG, RRK, LL, KG, FJ

ORCID

Haruki Hasegawa http://orcid.org/0000-0002-3464-4715
Randal R. Ketchem http://orcid.org/0000-0002-7821-2682
Frederick Jacobsen http://orcid.org/0000-0003-3594-9251

References

[1] Glaus A. Uber multiples myelozytom mit egnartigen, zum teil cristallahnlichen zelleingnlagerungen kombiniert mit elastolyse und ausgedehnter amyloidose und verkalkung. Virchows Arch Pathol Anatomical Record. 1917;223:301-39. doi:10.1007/BF02034325
[2] White RG. Observations on the formation and nature of Russell bodies. British journal of experimental pathology. 1954;35:365-76. PMID:13190123
[3] Goldberg AF, Deane HW. A comparative study of some staining properties of crystals in a lympho-plasmocytoid cell, of Russell bodies in plasmocytes, and of amyloids–with special emphasis on their isoelectric points. Blood. 1960;16:1708-21. PMID:13706437
[4] Goldberg AF. An unusual lymphomatous disease associated with intracytoplasmic crystals in lymphoplasmocytoid cells, Blood. 1960;16:1693-1707. PMID:13706439
[5] Agashe SR, Pol JN, Kadkol GA, Patil PP. Crystalline inclusions in myeloma cells: Need to go beyond morphologic curiosity. Indian journal of pathology & microbiology. 2017;60:139-40.
[6] Hasegawa H. Aggregates, crystals, gels, and amyloids: intracellular and extracellular phenotypes at the crossroads of immunoglobulin physicochemical property and cell physiology. International journal of cell biology. 2013;2013:604867. doi:10.1155/2013/604867. PMID:23533417
[7] Jack HM, Sloan B, Grisham G, Reason D, Wabl M. Large cytoplasmic inclusion body kappa-chain has unusual intrachain disulfide bonding. J Immunol. 1993;150:4928-33. PMID:8388424
[8] Shultz LD, Coman DR, Lyons BL, Sidman CL, Taylor S. Development of plasmacytoid cells with Russell bodies in autoimmune "viable motheaten" mice. The American journal of pathology. 1987;127:38-50. PMID:3551623
[9] Hurez D, Flandrin G, Preud'homme JL, Seligmann M. Unreleased intracellular monoclonal macroglobulin in chronic lymphocytic leukaemia. Clinical and experimental immunology. 1972;10:223-34.
[10] Cawley JC, Barker CR, Britchford RD, Smith JL. Intracellular IgA immunoglobulin crystals in chronic lymphocytic leukaemia. Clinical and experimental immunology. 1973;13:407-16.
[11] Feremans WW, Neve P, Caudron M. IgM lambda cytoplasmic crystals in three cases of immunocytoma: a clinical, cytochemical, and ultrastructural study. Journal of clinical pathology. 1978;31:250-8. doi:10.1136/jcp.31.3.250. PMID:417092
[12] Ralfkiaer E, Hou-Jensen K, Geisler C, Plesner T, Henschel A, Hansen MM. Cytoplasmic inclusions in lymphocytes of chronic lymphocytic leukaemia. A report of 10 cases, Virchows Archiv. A, Pathological anatomy and histology. 1982;395:227-36.
[13] Stefani S, Chandra S, Schrek R, Tonaki H, Knospe WH. Endoplasmic reticulum–associated structures in lymphocytes from patients with chronic lymphocytic leukemia. Blood. 1977;50:125-39. PMID:194637
[14] Yamamoto T, Hishida A, Honda N, Ito I, Shirasawa H, Nagase M. Crystal-storing histiocytosis and crystalline tissue deposition in multiple myeloma. Archives of pathology & laboratory medicine. 1991;115:351-4.
[15] Schaefer HE. Gammopathy-related crystal-storing histiocytosis, pseudo- and pseudo-pseudo-Gaucher cells. Critical commentary and mini-review, Pathology, research and practice. 1996;192:1152-62. doi:10.1016/S0344-0338(96)80037-9
[16] Rengers JU, Touchard G, Decourt C, Deret S, Michel H, Cogne M. Heavy and light chain primary structures control IgG3 nephritogenicity in an experimental model for cryocrystalglobulinemia, Blood. 2000;95:3467-72. PMID:10828030
[17] Hasegawa H, Wendling J, He F, Trilisky E, Stevenson R, Franey H, Kinderman F, Li G, Piedmonte DM, Osslund T, Shen M, Ketchem RR. In vivo crystallization of human IgG in the endoplasmic reticulum of engineered Chinese hamster ovary (CHO) cells. The Journal of biological chemistry. 2011;286:19917-31. doi:10.1074/jbc.M110.204362. PMID:21464137
[18] Hasegawa H, Forte C, Barber I, Turnbaugh S, Stoops J, Shen M, Lim AC. Modulation of in vivo IgG crystallization in the secretory pathway by heavy chain isotype class switching and N-linked glycosylation. Biochimica et biophysica acta. 2014;1843;1325-38.
[19] He F, Becker GW, Litowski JR, Narhi LO, Brems DN, Razinkov VI. High-throughput dynamic light scattering method for measuring viscosity of concentrated protein solutions, Analytical biochemistry. 2010;399:141-3.
[20] Wypych J, Li M, Guo A, Zhang Z, Martinez T, Allen MJ, Fodor S, Kelner DN, Flynn GC, Liu YD, Bondarenko PV, Ricci MS, Dillon TM, Balland A. Human IgG2 antibodies display disulfide-mediated structural isoforms. The Journal of biological chemistry. 2008;283:16194-16205. doi:10.1074/jbc.M709987200. PMID:18339624
[21] Stoops J, Byrd S, Hasegawa H. Russell body inducing threshold depends on the variable domain sequences of individual human IgG clones and the cellular protein homeostasis. Biochimica et biophysica acta. 2012;1823:1643-57. doi:10.1016/j.bbamcr.2012.06.015. PMID:22728328
[22] McCann SR, Whelan A, Greally J. Intracellular lambda light chain inclusions in chronic lymphocytic leukaemia. British journal of haematology. 1978;38:367-71. doi:10.1111/j.1365-2141.1978.tb01056.x. PMID:205239
[23] Reason DC. A murine hybridoma with large cytoplasmic inclusions of kappa light chains. The Journal of experimental medicine. 1987;165:578-583. doi:10.1084/jem.165.2.578. PMID:3029271
[24] Hasegawa H, Patel N, Lim AC. Overexpression of cryoglobulin-like single-chain antibody induces morular cell phenotype via liquid-liquid phase separation in the secretory pathway organelles. The FEBS journal. 2015;282:2777-95. doi:10.1111/febs.13332. PMID:26036200
[25] Stich MH, Swiller AI, Morrison M. The grape cell of multiple myeloma. American journal of clinical pathology. 1955;25:601-602. PMID:14361356
[26] Hasegawa H, Hsu A, Tinberg CE, Siegler KE, Nazarian AA, Tsai MM. Single amino acid substitution in LC-CDR1 induces Russell body phenotype that attenuates cellular protein synthesis through eIF2alpha phosphorylation and thereby downregulates IgG secretion despite operational secretory pathway traffic. mAbs. 2017;9:854-873; PMID: 28379093
[27] Hasegawa H, Woods CE, Kinderman F, He F, Lim AC. Russell body phenotype is preferentially induced by IgG mAb clones with high intrinsic condensation propensity: relations between the biosynthetic events in the ER and solution behaviors in vitro. mAbs. 2014;6:1518-1532. doi:10.4161/mabs.36242. PMID:25484054
[28] Paroutis P, Touret N, Grinstein S. The pH of the secretory pathway: measurement, determinants, and regulation. Physiology. 2004;19:207-15. doi:10.1152/physiol.00005.2004. PMID:15304635
[29] Yadav S, Laue TM, Kalonia DS, Singh SN, Shire SJ. The influence of charge distribution on self-association and viscosity behavior of monoclonal antibody solutions. Molecular pharmaceutics. 2012;9:791-802.
[30] Yadav S, Sreedhara A, Kanai S, Liu J, Lien S, Lowman H, Kalonia DS, Shire SJ. Establishing a link between amino acid sequences and self-associating and viscoelastic behavior of two closely related monoclonal antibodies. Pharmaceutical research. 2011;28:1750-64. doi:10.1007/s11095-011-0410-0. PMID:21626060
[31] Orsi A, Bakunts A, Lari F, Tadè L, Cattaneo A, Sitia R, Raimondi A, Bachi A, van Anken E, Vitale M. The unfolded protein response turns from pro-survival to pro-death to cap the extent of endoplasmic reticulum expansion. bioRxiv. 2017. [Advance online publication]. https://doi.org/10.1101/134726
[32] Berman HM, Westbrook J, Feng Z, Gilliland G, Bhat TN, Weissig H, Shindyalov IN, Bourne PE. The Protein Data Bank. Nucleic acids research. 2000;28:235-42. doi:10.1093/nar/28.1.235. PMID:10592235
[33] Honegger A, Pluckthun A. Yet another numbering scheme for immunoglobulin variable domains: an automatic modeling and analysis tool. Journal of molecular biology. 2001;309:657-70. doi:10.1006/jmbi.2001.4662. PMID:11397087